J Mater Sci (2007) 42:5722–5727
DOI 10.1007/s10853-006-0658-7

Morphology, microstructure, and residual stress in EBPVD erbia coatings

Alan F. Jankowski · Cheng K. Saw · James L. Ferreira · Jennifer S. Harper · Jeffrey P. Hayes · Bruce A. Pint

Received: 30 January 2006 / Accepted: 10 July 2006 / Published online: 21 April 2007
© Springer Science+Business Media, LLC 2007

Abstract The electron-beam physical vapor deposition of erbium-oxide coatings onto sapphire wafers is investigated to evaluate processing effects on the residual stress state and microstructure. The erbium-oxide coatings are found to be in a compressive stress state. The crystallographic texture of the erbium-oxide coating is evaluated using X-ray diffraction along with an assessment of forming the cubic erbia phase as a function of substrate temperature. In addition to the cubic erbia phase, an orthorhombic phase is found at the lower deposition temperatures. A transition is found from a two-phase erbium-oxide coating to a single phase at deposition temperatures above 948 K. The variation in morphology with deposition temperature observed in fracture cross-sections is consistent with features of the classic zone growth models for vapor-deposited oxide coatings. For high-temperature applications, a deposition process temperature above 948 K is seen to produce a stoichiometric, fully dense, and equiaxed-polycrystalline coating of cubic erbia.

Introduction

The physical vapor deposition (PVD) of erbia coatings is of interest in several technologies. For instance, in a magnetic confinement fusion reactor, a thick electrically insulating coating of erbia can reduce the pressure drop due to magneto-hydro dynamic (MHD) force [1–3]. As a thin coating, erbia may be a reasonable substitute for silica [4, 5] as a gate dielectric. Erbia can be grown as well by methods other than PVD. For example, an organometallic chemical vapor deposition has been assessed [6] as a protective coating to resist corrosion by liquid metals. Again for the application of corrosion protection when immersed in molten metals, a plasma ion implantation of erbium metal ions followed by growth of erbium oxide has been studied [7, 8] to assess improvement of adherence of the ceramic coating to various substrate surfaces. Erbia deposited by plasma-assisted physical vapor deposition using a filtered arc device has been studied [9] a barrier coating to hydrogen permeation.

The sampling of literature related to the PVD of erbia coatings is somewhat limited [4, 5, 9] to the growth of thin coatings, i.e. less than a micron thick. Thick coatings are being investigated to provide a reliable long-term solution to the MHD problem [1–3] in fusion reactors. For this application, an electrically insulating barrier is needed to decouple the liquid metal coolant (e.g. lithium) from the metal (e.g. a vanadium alloy) flow channel wall to minimize the MHD force which inhibits the liquid metal from flowing across the magnetic field lines. For a lithium cooled blanket operating at temperatures up to 1,000 K, only very-stable oxides are being considered [10], as lithium will dissolve most oxides at high temperature. Some results obtained for electron-beam physical vapor deposition (EBPVD) of yttria coatings [10] are promising as little change is measured in resistivity from the as-deposited condition after exposure to liquid lithium at 973 K, wherein values remain above the lower bound limit for coatings of 10^5 to 10^6 Ω-cm. As an alternative to yttria,

A. F. Jankowski (✉) · C. K. Saw · J. L. Ferreira · J. S. Harper · J. P. Hayes
Materials Science and Technology Division, Lawrence Livermore National Laboratory, Mail Stop L-352, P.O. Box 808, Livermore, CA 94550, USA
e-mail: alan.jankowski@ttu.edu

B. A. Pint
Metals and Ceramics Division, Oak Ridge National Laboratory, P.O. Box 2008, Oak Ridge, TN 37831, USA

we now present results on the preparation and characterization of EBPVD erbia coatings for use at temperatures above 973 K.

The thermal history of the EBPVD process is important not only for application at high temperatures (above 973 K) but for the microstructure produced in the coating. That is, the morphology and phase stability of oxide coatings evaporatively deposited from stoichiometric targets are dependent upon the incident electron-beam power and the substrate temperature. Too high a target power density can lead to an oxygen deficiency in the vapor, and too low a substrate temperature leads to an under-dense porous coating. Often a compressive residual stress state is considered beneficial for adhesion. However, it is generally understood [11] that too large a magnitude of compressive stress can lead to decohesion of the coating from its substrate. These features are investigated in the present study of EBPVD erbia coatings.

Experimentals

Erbium-oxide coatings that are 1–10 μm in thickness are fabricated using the EBPVD process. The target material for the evaporation is a hot-pressed erbia-powder compact at 82.1 ± 0.6% full density, i.e. 7.09 ± 0.05 gm cm^{-3}. The evaporation source consists of only the cubic erbia phase as confirmed by X-ray diffraction analysis. The electron-beam is operated at 8–10 kV and is rastered over 1–2 cm^2 of target surface yielding a beam current density of 25–100 mA cm^{-2}. The evaporation source-to-substrate separation is 10–15 cm. The vapor pressure during deposition is ~1 mPa. Evaporation rates up to 20 nm s^{-1} are produced under these conditions. The C-cut (00.2) sapphire-wafer substrates are heated from the reverse using quartz lamps. The coating temperature is monitored using thermocouples placed in direct contact with the obverse side of the substrate. The coating temperature is influenced by the amount of heat generated from the evaporative melt with a typical rise of 20–30 K above the preheat temperature, and then equilibrates to a isothermal value within two minutes of exposure. A substrate temperature range of 600–1,100 K is used in this study.

The microstructure of the as-deposited coating is examined using scanning electron microscopy (SEM) and X-ray diffraction (XRD). The growth morphology of the erbium-oxide coating is imaged in cross-section using a SEM. The crystallographic texture of any erbium-oxide phases present in the as-deposited coatings are characterized using XRD. A double crystal diffractometer using monochromatic Cu kα radiation in the $\theta/2\theta$ mode reveals the intensity of diffracted reflections over a 2θ range of 10–70°. The crystal structure and phase of a free-standing, low-temperature erbium oxide deposit is examined in plan view using transmission electron microscopy (TEM) with bright field imaging and selected-area diffraction. The curvature of the coated substrate, as measured using contact profilometry, is used to compute the residual stress state.

Results and analysis

Morphology and microstructure

The growth morphologies of the erbium-oxide coatings are shown in fracture cross-section using SEM images. The images of Fig. 1 correspond with a sampling of coatings deposited over a temperature range of 24–36% of the erbia melt point at 2,673 K. A transition in the morphology with

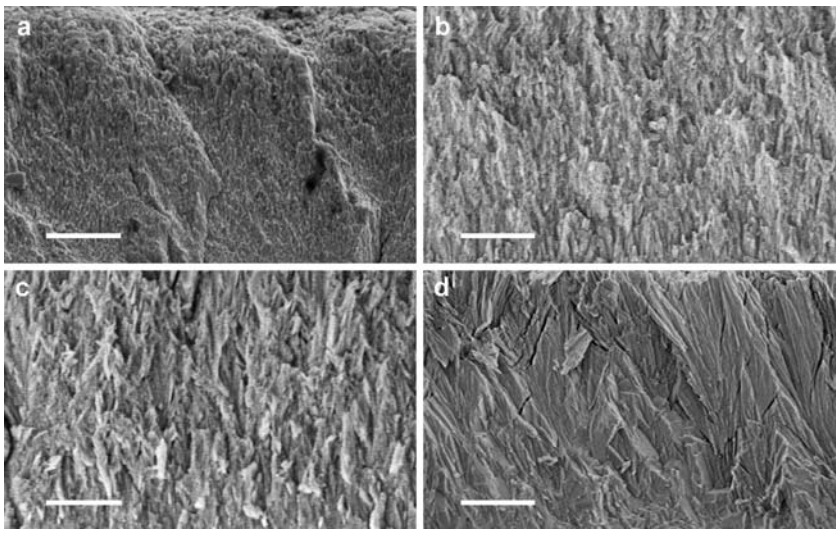

Fig. 1 The growth morphology of erbium-oxide coatings are revealed in cross-section as deposited on sapphire wafers at temperatures of (**a**) 665 K, (**b**) 758 K, (**c**) 853 K, and (**d**) 948 K. The scale marker is 2 μm in length

coating temperature is seen from features of densely packed fibrous grains (in Fig. 1a) at 665 K through columnar grains (in Fig. 1b–c) at 758-to–853 K, to the onset of a recrystallized grain structure (in Fig. 1d) at 948 K. The effect of temperature on structural zones is well described [12–14] in growth models for metal and oxide condensates. The evolution in morphologies observed in the present study is consistent [12] with the typical temperature range that bounds Zone 2, i.e. columnar grain growth, for PVD oxides.

The atomic positions fit to the powder diffraction data (PDF file no. 43-1007) for the erbia phase of Er_2O_3 [15] yield a cubic structure with a lattice parameter of 1.055 nm. The ceramic erbium-oxide coatings have a characteristic pink color. A least squares fit of the powder diffraction data (PDF file no. 42-0725) for an erbium-formate hydrate phase of $C_3H_3ErO_6 \cdot 2H_2O$ yields [16] an orthorhombic structure with lattice parameters of 0.833, 1.224, and 0.747 nm. The majority of the XRD peaks seen in Fig. 2 fit the cubic phase as demarcated by solid diamond symbols along with the respective Miller indices. The log scale plot of Fig. 2 highlights the intensity of non-cubic phase reflections for use in identification. The remaining peaks demarcated by open diamond symbols at the 2θ positions of 15.9°, 30.8°, 32.5°, 33.4°, 43.5°, 49.9°, and 52.8° can all be indexed to an orthorhombic phase (with lattice parameters equivalent to the erbium hydrate phase) with likely corresponding indices of (101), (122), (202), (141), (322), (260), and (124). The powder diffraction data (PDF file no. 02-0930) for the hexagonal structure of erbium metal or that of the corundum sapphire substrate can not be used to account for the additional diffraction peaks in Fig. 2 that are not indexed to cubic erbia. The

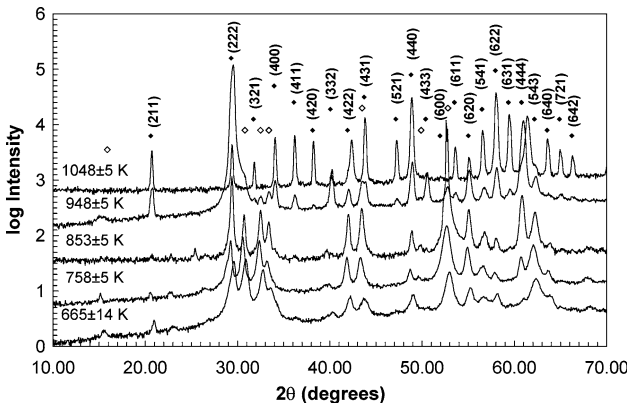

Fig. 2 The Cu Kα X-ray diffraction scans of erbium-oxide coatings taken in the $\theta/2\theta$ mode are shown as deposited at temperatures of (**a**) 665 K, (**b**) 758 K, (**c**) 853 K, (**d**) 948 K, and (**e**) 1,048 K. The 2θ positions of the Bragg reflections for the cubic phase of erbia Er_2O_3 are marked by the *solid diamonds* whereas reflections that do not match the cubic phase are marked by *open diamonds*

intensity of the Bragg reflections for the orthorhombic phase appears to progressively decrease as the coating temperature increases. Above 948 K (and certainly by 1,048 K), only the cubic erbia phase is observed in the as-deposited coating. The higher deposition temperature is consistent with surpassing the 897–923 K melt point (or decomposition) range that can be typical of hydrate-type orthorhombic phases.

Transmission electron microscopy of the 853 K erbium oxide deposit is pursued to confirm evidence seen in Fig. 2 XRD scans of a non-cubic erbium-oxide phase. The bright field TEM image in Fig. 3a reveals a fine (submicron) grain microstructure. Some phase contrast appears in the high magnification image revealing dark features that are ~10–25 nm in size. In the corresponding diffraction pattern of Fig. 3b, taken using a long camera length, a second diffracting phase is clearly identifiable. The continuous dark circles are used to overlay the ring pattern attributable to the cubic erbia phase. The arrows in Fig. 3b point to the additional reflections that fit the orthorhombic phase. These interplanar spacings match the (122), (202), and (141) Bragg reflections of the orthorhombic phase as seen in Fig. 2 for the 853 K erbium-oxide deposit. However, it is not certain that the contrasted features of the Fig. 3a bright field imaging are attributable to an erbium oxide phase other than the cubic erbia phase. The proximity of the additional reflections (marked by the arrows) to the diffraction spots of the cubic phase (in Fig. 3b) preclude definitive matching of the orthorhombic phase using the dark field imaging mode.

Residual stresses

The residual film stress (σ) arises from structural and deposition processing effects. The stress risers include morphological and microstructure features, crystalline phase, and thermal transients during deposition. The residual stress state in the erbium-oxide coatings is computed using formulations developed [17–25] for assessing the convex-to-concave deflection of the coating-substrate system. Descriptions of stresses in thin films on beams [17] have been expanded to consider thick films on substrates [18], thin films on plates [19], and multilayer thick films on thick substrates [20–23]. The analysis methods are based on a strength-of-materials approach. For the case of an adherent thin film to a thick substrate, the biaxial equivalent [18, 23–25] of the thin film/beam case [17] suffices. The substrate assumes a radius (R) of curvature under the combined force resulting from the intrinsic and extrinsic stresses [11] that are induced during the deposition. For the condition that the deformation of the coating and substrate is elastic, the biaxial stress in the film (σ) is given by the expression:

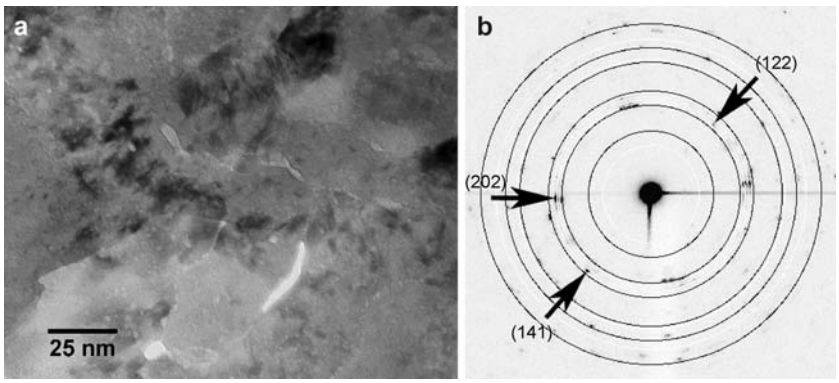

Fig. 3 Transmission electron microscopy of a 853 K erbium oxide reveals (**a**) the microstructure as a bright field image, and (**b**) the crystalline phase as a selected-area diffraction pattern

$$\sigma = E_s[6(1-\nu_s)]^{-1}(t_s)^2(t)^{-1}(R)^{-1} \quad (1)$$

where the coating thickness (t) is much less than the substrate thickness (t_s). The Young's modulus (E_s) and Poisson's ratio (ν_s) of the substrate are constants. For the present case of an oriented sapphire substrate, the Young's modulus can be computed [26] from tabulated values [27] of elastic compliances (S_{ij}). Using the rhomobohedral Miller indice (hkl) equivalence [28] of (012) for corundum sapphire Al_2O_3, the value computed for E_s is 520 GPa. This value is near equivalent to the 524 GPa Young's modulus value determined for sapphire whiskers [29]. The Poisson ratio ν_s is estimated as 0.16. The radius (R) of curvature to be input to Eq. 1 is computed [30] from the height (Δh) of the coating-substrate deflection over a cord radius (r) using the expression:

$$\Delta h = r^2(2R)^{-1} \quad (2)$$

The height (Δh) of the deflection is taken as the difference between that measured for the coated substrate minus that value for an uncoated substrate at each deposition temperature. The deflection of the coated substrate is measured using a contact profilometer along a 10 mm trace, i.e. a radius (r) of 5 mm. Three or more traces are taken at each of two orthogonal positions.

The results for film stress in erbium-oxide coatings deposited on sapphire wafers are listed in Table 1. The variation of film stress with coating temperature is plotted in Fig. 4. The stress state is modeled as a function of deposition temperature from the average vertical deflection of the coating-substrate as computed from measurements along the orthogonal traces. A curve fit to trend the experimental measurements using a second-order polynomial expression is

$$\sigma_f = -3,100 + 7.1T - 0.0041T^2 \quad (3)$$

where the unit of stress (σ_f) is MPa and the unit of temperature (T) is K. The curve for Eq. 3 is plotted in Fig. 4 along with the stress results obtained from deflection measurements using Eqs. 1 and 2 with the data listed in Table 1.

Discussion

The morphology in erbium-oxide coatings observed (in Fig. 1) over the experimental temperature range is that of a dense structure shifting from a columnar to equiaxed type growth as is consistent with the zone models [12–14] for PVD growth. We find that the erbium-oxide coatings are crystalline at all deposition temperatures examined, i.e. down through 600 K. Many deposition studies [5, 9] indicate lack of a well-defined as-deposited crystalline erbium oxide below deposition temperatures of ~800 K. Our X-ray diffraction results show, in general, a randomly

Table 1 Dimensions and deflection of erbia-coated sapphire wafers

Coating temperature, T (K)	Substrate thickness, t_s (μm)	Coating thickness, t (μm)	Net height of deflection Δh (μm)	Film stress, σ (MPa)
665	508	9.16 ± 0.41	–0.817 ± 0.075	–189 ± 27
718	406	4.97 ± 0.38	–0.261 ± 0.086	–71 ± 31
758	406	11.78 ± 0.58	–0.878 ± 0.082	–101 ± 15
853	508	8.62 ± 0.71	–0.189 ± 0.064	–47 ± 21
873	406	2.99 ± 0.21	+0.024 ± 0.053	11 ± 27
948	406	8.19 ± 0.26	–0.455 ± 0.094	–75 ± 18
970	508	4.03 ± 0.17	–0.170 ± 0.069	–91 ± 42
988	508	1.14 ± 0.05	–0.044 ± 0.023	–82 ± 48

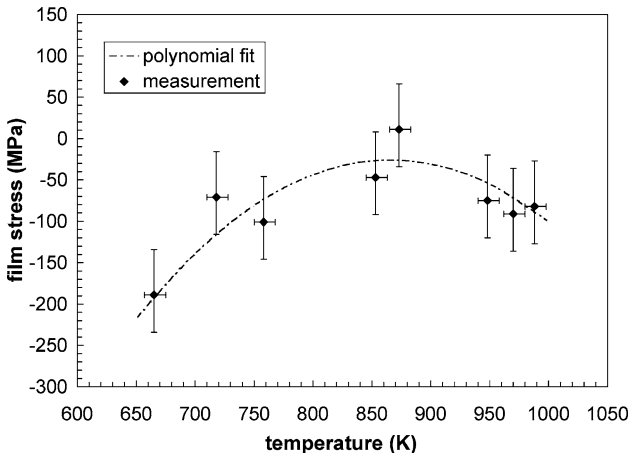

Fig. 4 The residual stress (MPa) for erbium-oxide coatings deposited on sapphire wafers at temperature (K) as computed from averaged deflection measurements along orthogonal traces along with a best-fit polynomial curve

oriented growth but with evidence of a two-phase structure for low deposition temperatures. The non-cubic erbium-oxide phase is confirmed with electron diffraction for the 853 K deposit. This result is not obvious for the case [4] of <0.1 μm-thin, low-temperature EBPVD coatings of erbia that are annealed wherein a preferred (111) texture of the cubic phase is observed. Evidence for a non-cubic erbium-oxide phase is seen in the X-ray diffraction scans for e-beam and plasma-assisted PVD coatings [9, 31, 32] deposited at temperatures below 948 K. The present two-phase structure reduces to that of only erbia at temperatures above 948 K. The other low-temperature phase appears to be consistent with a lower melt-point orthorhombic erbium-oxide phase, such as the ErO_6 phase. At present, the low-temperature orthorhombic phase may originate from the nature of the source material for the EBPVD process. That is, the erbia target compact is not fully dense but contains trapped porosity. It is possible that the additional elements (of hydrogen and oxygen) needed to produce an orthorhombic hydrate-type phase come from the internal pores wherein trapped moisture may reside. For the cases of reactive deposition [31, 32] at temperatures below 948 K, a partial pressure of oxygen is added during the coating process.

The residual stress state does not appear to correlate with the absolute film thickness (for the data listed in Table 1) but rather stress varies with the coating temperature. Thus, the residual stress state of the erbium oxide coatings is represented in Eq. 3 as a function of temperature. However, there are both growth morphological and temperature effects that comprise the intrinsic and extrinsic features of residual stress, respectively. The merits of contributions from each effect will be discussed separately with remarks given as to the dominant effect for high-temperature growth.

The erbium-oxide film stress is in compression at low deposition temperature, shifts under a tensile effect towards stress neutral as the temperature increases to ~875 K, and then shifts again into compression as the temperature continues to increase. The stress state change can be attributed to the change in the coefficient of thermal expansion (CTE) for the coating as based on the two phases present in the coating and how the phase content changes with increased temperature. The assumption is that the mixed phase coating has a CTE smaller than that of the sapphire substrate at 8.0×10^{-6} $(°C)^{-1}$ and perhaps less than that for the cubic erbia phase as well. At the lowest deposition temperature where the second (orthorhombic) phase is most prominent, a compressive residual stress state results. The orthorhombic erbium-oxide phase causes the coating to contract less than the sapphire. As the temperature increases, the second phase is reduced and then diminished in content. If the CTE of the coating increases towards the value of sapphire, then the compressive stress state is reduced. That is, the low-temperature compressive state moves towards stress neutral with an increase in temperature. As the deposition temperature increases beyond 948 K, the orthorhombic phase is certainly no longer present and the coating shifts towards compression again. Beyond 900 K, the coating CTE is likely slightly less than that for the sapphire substrate.

In another scenario, if a coating CTE is assumed near equivalent to the sapphire substrate, then the coating stress state would have to be attributable to changes in morphology. In this case, a shift from fibrous grains through a columnar to equiaxed type growth would be associated with a change from a deposition-induced tensile to compressive residual-stress state. This transition follows a change in the net deformation of the coating-substrate deflection from concave to convex. The low temperature coating would be in a tensile-like state if the morphology was of an under-dense columnar type, incapable of supporting in-plane stress. The higher coating temperatures would be associated with a fully dense structure capable of supporting compressive stresses. The morphological effect on stress is consistent with the erbia coatings deposited at higher temperatures, i.e. greater than 948 K.

Therefore, it follows that the dominant effect in the residual stress state of the erbia coatings above the 948 K deposition temperature can be directly attributable to the difference in the CTE between the substrate and the coating as is consistent with the effects of morphological features. For example, using Eq. 3 to compute a residual compressive stress of 100 MPa for a 1,000 K deposition temperature, an approximate value for the CTE of erbia follows as ~7.7×10^{-6} $(°C)^{-1}$ assuming a modulus of 0.5 TPa.

Summary

Erbium-oxide coatings are deposited on sapphire wafers using the electron-beam evaporation of a hot-pressed erbia compact over a temperature range of 600–1,100 K. In cross-section, SEM images show the coatings to have columnar and equiaxed growth depending on the deposition temperature. XRD and TEM revealed a polycrystalline oxide coating consisting of stoichiometric cubic erbia (Er_2O_3). In addition, the presence of a second orthorhombic phase (ErO_6) is found when the deposition temperature was less than 948 K. A compressive stress state was measured at room temperature in the erbium-oxide coatings deposited onto sapphire substrates at all deposition temperatures. However, there appeared a minimum magnitude in stress at 870 K. A compressive stress state in fully dense coatings is favorable, both for adherence and full protection of the underlying substrate. The residual stress in the erbia coatings was small at ~100 MPa compression for deposition temperatures above 948 K. Deposition at temperatures above 948 K yields just the cubic erbia phase, avoiding potential shortcomings of the presence of an additional unstable orthorhombic erbium-oxide phase that is seen in coatings grown at lower deposition temperatures. As consistent with the deformation mode of the erbium-oxide coated sapphire wafers and the growth morphology observed in the erbia coating above 948 K, the residual stress measurements above 950 K suggest a CTE of ~7.7×10^{-6} $(°C)^{-1}$ for erbia that is less than the 8.0×10^{-6} $(°C)^{-1}$ value for sapphire. The growth condition to produce pure erbia in coatings at deposition temperature >948 K would be preferable to evaluate its performance under MHD applications wherein an adherent and stable oxide coating (as deposited on metal substrates like vanadium alloy) would be exposed to liquid lithium at temperatures above 973 K. The synthesis of cubic erbia coatings by alternative PVD techniques, such as arc-source plasma assisted deposition, can be considered provided the coatings are deposited at elevated temperature to avoid the formation of unstable second phases, and to be compatible with the intended high-temperature application.

Acknowledgements The research was sponsored by the Office of Fusion Energy Sciences, U.S. Department of Energy and by the US-Japan JUPITER-II collaboration with the MHD coating subtask led by Prof. T. Muroga, NIFS (Natl. Institute for Fusion Science). This work was performed under the auspices of the U.S. Department of Energy by the University of California, Lawrence Livermore National Laboratory under Contract No. W-7405-Eng-48.

References

1. Barleon L, Casal V, Lenhart L (1991) Fusion Eng Design 14:401
2. Malang S, Borgstedt HU, Farnum EH, Natesan K, Vitkovski IV (1995) Fusion Eng Design 27:570
3. Park JH, Kassner TF (1996) J Nucl Mater 233–237:476
4. Mikhelashvili V, Eisenstein G, Edelmann F (2002) Appl Phys Lett 80:2156
5. Singh MP, Thakur CS, Shalini K, Bhat N, Shivashankar SA (2003) Appl Phys Lett 83:2889
6. Hubbard KM, Espinoza BF (2000) Thin Solid Films 366:175
7. Wood BP, Reass WA, Henins I (1996) Surf Coatings Technol 85:70
8. Walter KC, Nastasi M, Baker NP, Munson CP, Scarborough WK, Scheuer JT, Wood BP, Conrad JR, Sridharan K, Malik S, Bruen RA (1998) Surf Coatings Technol 103–104:205
9. Koch F, Brill R, Maier H, Levchuk D, Suzuki A, Muroga T, Bolt H (2004) J Nucl Mater 329–333:1403
10. Pint BA, Tortorelli PF, Jankowski A, Hayes J, Muroga T, Suzuki A, Yeliseyeva OI, Chernov VM (2004) J Nucl Mater 329–333:119
11. Campbell DS (1970) In: Maissel L, Glang R (eds) Handbook of thin film technology (Ch. 12). McGraw-Hill, New York
12. Movchan BA, Demchishin AV (1969) Fizika Metall 28:653
13. Bunshah RF, Juntz RS (1973) Met Trans 4:21
14. Colen M, Bunshah RF (1976) J Vac Sci Technol 13:536
15. Saiki A (1985) J Ceram Assoc Jpn 93:649
16. Wenk H-R (1981) Z Kristallogr 154:137
17. Stoney GG (1909) Proc R Soc Lond Ser A 82:172
18. Brenner A, Senderoff S (1949) J Res Nat Bur Stand 42:105
19. Hoffman RW (1966) Phys Thin Films 3:211
20. Saul RH (1969) J Appl Phys 40:3273
21. Olsen GH, Ettenberg M (1977) J Appl Phys 48:2543
22. Vilms J, Kerps D (1982) J Appl Phys 53:1536
23. Townsend PH, Barnett DM, Brunner TA (1987) J Appl Phys 62:4438
24. Henein GE, Wagner WR (1983) J Appl Phys 54:6395
25. Jankowski A, Bionta F, Gabriele P (1989) J Vac Sci Technol A7:210
26. Nye JF (1960) Physical properties of crystals. Clarendon, Oxford, p 131
27. Trent HM, Stone DE, Beaubien LA (1982) In: Gray DE (ed) American Institute of Physics handbook (3rd ed). McGraw-Hill, New York, p. 55
28. Huang T, Parrish W, Masciocchi N, Wang P (1990) Adv X-Ray Anal 33:295
29. CRC (1985) In: Weast RC, Astle MJ, Beyer WH (eds) Handbook of chemistry and physics (65th ed). CRC Press, Boca Raton, p F-59
30. Jankowski AF, Hayes JP, Felter TE, Evans C, Nelson AJ (2002) Thin Solid Films 420–421:43
31. Sawada A, Suzuki A, Maier H, Koch F, Terai T, Muroga T (2005) Fusion Eng Design 75–79:737
32. Adams RO, Digiallonardo A, Nordin CW (1987) Thin Solid Films 154:101